Influence of multiple electron scattering on the gain in a gas-loaded free-electron laser

V. V. Goloviznin* and P. W. van Amersfoort
FOM–Instituut voor Plasmafysica "Rijnhuizen," P.O. Box 1207, 3430 BE Nieuwegein, The Netherlands
(Received 28 November 1994)

We present an analysis of the small-signal gain in the gas-loaded free-electron laser. Multiple scattering of electrons by the atoms of the gas inside the optical cavity is shown to lead to two additional effects, as compared to the case of a vacuum free-electron laser: a loss of coherence between different parts of the electron trajectory and an enhancement of the phase "jitter." Both effects become increasingly important at short wavelengths and significantly reduce the small-signal gain per pass. In one-dimensional approximation, analytical expressions are obtained and numerical calculations are made to estimate the beam and undulator parameters necessary for lasing in the vacuum ultraviolet.

PACS number(s): 41.60.Cr

I. INTRODUCTION

The free-electron laser (FEL) uses a beam of relativistic electrons traveling through a periodic magnetic structure, the so-called undulator, to generate an intense, coherent electromagnetic wave at a frequency that is determined by the electron energy and by the period and field strength of the undulator [1]. There is a growing awareness that there are two important "niches" for the FEL as a scientific research tool: the far-infrared spectral range above roughly 10 μm and the vacuum ultraviolet (VUV) below 200 nm [2]. This is related to the absence of regular (intense) lasers in these parts of the spectrum.

In the IR, FEL technology has reached the level of maturity and cost effectiveness that permits operation as a user facility. The situation is different in the VUV and beyond, first because of the much higher electron energy that is required (typically several hundred MeV up to several GeV, instead of several tens of MeV), second because the gain falls off dramatically, and third because optics becomes a serious problem. It is worth noting that, in this part of the spectrum, ordinary lasers also face strong limitations due to the "Einstein collapse," which makes it increasingly difficult to create and maintain a population inversion as the photon energy increases.

It was proposed by Fauchet *et al.* to relax requirements on electron energy by the introduction of a gas into the optical cavity [3]. The main idea is that this reduces the phase velocity of the electromagnetic wave, and, therefore, FEL resonance occurs at a shorter wavelength. For relatively small deviations from the vacuum wavelength, this was confirmed in experiments performed at Stanford University [4–6]. When the pressure is properly adjusted, the gas may provide a considerably larger upshift—typically one or two orders of magnitude—of the laser frequency [7–9]. This makes the gas-loaded FEL a promising candidate for operation in the VUV at the electron energies that nowadays are used for operation in the IR.

Unfortunately, the gas inside the cavity not only slows down electromagnetic waves but also "damages" the electron beam as it passes through the interaction area. The scattering of electrons by the gas is an important feature of the gas-loaded FEL (GFEL). A theoretical analysis of the small-signal gain in a GFEL including multiple scattering effects was made in [8]. The analysis was based on the assumption that the scattering can be represented as a degradation of the initial beam emittance.

In the present paper, we study the influence of multiple scattering on the small-signal gain in a GFEL in a more detailed way. First, we take into account a possible loss of coherence between different parts of the trajectory of an electron inside the undulator. This effect is shown to be important in the short wavelength region where it leads to a significant gain reduction. Second, we include into the consideration a phase "jitter" due to a modulation of the longitudinal electron velocity. For conventional FEL's, it is well known that, in the case of a planar undulator, significant modulation can occur on a length scale of one undulator period, with the consequence of a high-frequency oscillation of the particle phase relative to the ponderomotive potential well [1]. This reduces the gain. The effect is known to be negligible for helical undulators [1] provided that the angular spread in the electron beam is sufficiently small [10]. In a GFEL, however, phase "jitter" becomes important even for a helical undulator [11], due to the strong reduction in wavelength.

Analytical expressions for the small-signal gain are obtained and numerical calculations are made to estimate the prospects of lasing in the VUV. Our results show that the approximation used in [8] becomes inadequate in the short wavelength region. It may considerably overestimate the gain if used outside the limits of its validity.

The paper is organized as follows. In Sec. II, we consider the phase "jitter" in a helical GFEL. Multiple scattering is incorporated into our calculations in Sec. III. Section IV contains numerical results and a comparison of our analytical expressions with a few simple limit-

*Present address: Kurchatov Institute of Atomic Energy, 123182 Moscow, Russia.

ing cases. A summary and conclusions are given in Sec. V.

II. PHASE "JITTER" IN A GFEL

We start from the usual pendulum equations (see, e.g., [12]) describing phase and energy evolution of an electron in the combined field of a helical undulator plus an electromagnetic wave. In the one-dimensional (1D) approximation one has

$$\frac{d\epsilon}{dz}=\frac{m^2\omega}{\epsilon}a_u a_s \sin\Phi \ , \tag{1}$$

$$\frac{d\Phi}{dz}=\omega\left[\frac{1}{v_z}-n\right]\pm\Omega \ , \tag{2}$$

where m is the electron mass, z is the particle coordinate along the undulator axis, Φ is the particle phase with respect to the ponderomotive potential well, ϵ and v_z are the particle energy and longitudinal velocity, ω and $a_s=eE_0/m\omega$ are the frequency of the wave and its normalized intensity, and $\Omega=2\pi/\lambda_u$ and $a_u=eB_0/m\Omega$ are the corresponding undulator frequency and the undulator parameter, respectively. Relativistic units $\hbar=c=1$ are used throughout this paper.

In the following, a_s is assumed to be small, so that all quantities under consideration can be expanded to the lowest nonvanishing order in a_s. As usual, the initial conditions for Eqs. (1) and (2) correspond to a nonmodulated beam at the entrance of the undulator: $\Phi_0\equiv\Phi(z=0)$ is uniformly distributed from 0 to 2π. The result may then be averaged over the initial electron energy ϵ_i with a weight function corresponding to the energy spread of the electron beam.

The above set of equations differs from the corresponding equations for a vacuum FEL in two aspects. First, Eq. (2) contains a new parameter n, the refractive index of the medium inside the optical cavity; for a vacuum FEL one should obviously take $n=1$. Second, there is "$\pm$" sign in front of Ω because in a GFEL two resonant modes are possible [7]: a phase slip mode for which the electron slips one optical wavelength per undulator period as in a vacuum FEL, and a phase advance mode for which the phase velocity of the electromagnetic wave is so small that the electron advances it by one wavelength per undulator period. In the present paper we shall consider only the phase slip mode, which corresponds to the "$-$" sign, because the phase advance mode requires a higher gas pressure inside the cavity and is, therefore, more sensitive for multiple scattering.

The refractive index n for gases is close to unity and may thus be written as

$$n=1+\frac{\chi'}{2} \ , \tag{3}$$

where χ' is the real part of the dielectric permittivity of the medium. It is ω dependent and for frequencies below the resonant one satisfies the condition $0<\chi'\ll 1$. For simplicity, in the present paper we adopt an approximate expression for χ', which corresponds to a single spectral line with oscillator strength equal to unity [13]

$$\chi'(\omega)\approx\frac{N}{N_{\rm STP}}\frac{A}{(1-\omega^2/\omega_0^2)} \ , \tag{4}$$

where $N/N_{\rm STP}$ is the ratio of the actual gas density and the density under STP conditions (STP = standard temperature and pressure: 0 °C, 1 atm), ω_0 is the resonant atomic frequency, and A is a gas-dependent constant. The two most important cases are helium and hydrogen; corresponding parameters are shown in Table I.

Further, for an ultrarelativistic particle ($\epsilon\gg m$) the longitudinal velocity is close to unity. Namely,

$$v_z\approx 1-\frac{1}{2\gamma^2}-\frac{v_t^2}{2} \ , \tag{5}$$

where $\mathbf{v}_t=\{v_x,v_y\}$ is the transverse velocity of the particle and $\gamma=\epsilon/m$ is the Lorentz factor. If the transverse part of the undulator field is $\mathbf{B}_t(z)=\{B_0\cos\Omega z,B_0\sin\Omega z\}$, then up to small terms proportional to a_s the transverse velocity is

$$\mathbf{v}_t(z)=\mathbf{v}_{0t}-\frac{e\mathbf{B}(z)}{m\gamma\omega} \ , \tag{6}$$

where $\mathbf{v}_{0t}=\{v_{0x},v_{0y}\}$ is the transverse velocity of the particle at the entrance of the undulator ($z=0$).

Taking into account Eqs. (3)–(6), one can rewrite Eq. (2) as

$$\frac{d\Phi}{dz}=\frac{\omega}{2}\left[\frac{(1+a_u^2)}{\gamma^2}-\frac{2a_u}{\gamma}(v_{0x}\cos\Omega z+v_{0y}\sin\Omega z)+v_{0t}^2-\chi'\right]-\Omega \ . \tag{7}$$

Together with Eq. (1), the above equation forms now the set of equations describing the particle dynamics in a helical gas-loaded FEL.

Equations (1) and (7) still contain terms of different time scales: "fast" oscillations such as $\cos(\Omega z)$ with typical frequency Ω and "slow evolution" terms with much lower frequencies. The next step is to average the equations over one undulator period. As a result of this averaging, one has (see Appendix A)

$$\frac{d\gamma}{dz}=\frac{\omega}{\gamma}a_u a_s J_0\left[\frac{\omega a_u v_{0t}}{\gamma\Omega}\right]\sin\left[\Phi-\frac{\omega a_u v_{0y}}{\gamma\Omega}\right] \ , \tag{8}$$

$$\frac{d\Phi}{dz}=\frac{\omega}{2}\left[\frac{(1+a_u^2)}{\gamma^2}+v_{0t}^2-\chi'\right]-\Omega \ , \tag{9}$$

TABLE I. Refractive and scattering properties of hydrogen and helium; ω_0 is the resonant atomic frequency, $\lambda_0\equiv 2\pi/\omega_0$ is the cutoff wavelength, R is the characteristic scattering length [see Eq. (22)].

Gas	A	$\hbar\omega_0$ (eV)	λ_0 (nm)	R (m)
H_2	2.8×10^{-4}	10.2	121.6	16
He	0.7×10^{-4}	21.2	58.4	12

where J_0 is the zeroth order Bessel function.

Up to now, we did not include multiple scattering in our model. Before doing this, we will briefly discuss the equations obtained. First, from Eq. (9) one can see a modification of the synchronism condition under the influence of a medium, as compared to the case of a vacuum FEL. Assuming the angular spread in the electron beam to be small, $v_{0t}^2 \ll \gamma^{-2}$, and taking $d\Phi/dz \approx 0$, one has

$$\omega = \frac{2\Omega}{(1+a_u^2)\gamma^{-2} - \chi'} . \tag{10}$$

When properly adjusted, the two terms in the denominator may nearly compensate each other, thus leading to a considerable upshift of the frequency generated; for STP conditions (see Table I) nearly full compensation takes place for beam energies in the range 50–100 MeV. In fact, one should solve Eqs. (10) and (4) simultaneously because χ' is a function of ω. The corresponding photon frequency ω then becomes a double-valued function of the gas density (or pressure, if one keeps the temperature constant) [7].

Second, a simple estimate of the importance of the phase "jitter" can be made. The "jitter" influence is described by the argument of the Bessel function,

$$x = \frac{\omega a_u v_{0t}}{\gamma\Omega} .$$

Substituting here ω from Eq. (10) and taking into account that typically $v_{0t} \ll \gamma^{-1}$, one has

$$x \ll \frac{2a_u}{1+a_u^2-\chi'\gamma^2} . \tag{11}$$

For an ordinary helical FEL ($\chi'=0$), the Bessel function argument is $x \ll 1$ because the undulator parameter a_u is typically about unity; the "jitter" influence is thus negligibly small in this case. But as a compensation of the positive and negative terms in the denominator of Eq. (11) [and the corresponding frequency upshift, see Eq. (10)] becomes noticeable, the right hand side of the above condition allows x to be larger than unity. The "jitter" becomes thus increasingly important in the short wavelength region of GFEL operation.

III. INFLUENCE OF MULTIPLE SCATTERING

When passing through a GFEL, relativistic electrons from an accelerator inevitably collide with the atoms of the gas inside the optical cavity. The influence of these collisions will be taken into account in this section. Because of the long-range nature of the Coulomb force of interaction, a fast charged particle in a medium experiences many random small-angle scatterings. The process of multiple scattering looks, therefore, as a diffusion process in transverse velocity phase space, while the energy of the particle remains nearly constant.

Equations (8) and (9) contain an explicit dependence on the initial transverse velocity of the electron $\mathbf{v}_{0t}$. To incorporate collisions into our calculations, we should now consider the transverse velocity of the particle as a "slowly" varying function of the coordinate z. This assumption is consistent with the averaging of the exact equations of motion over one undulator period made above. It only means that the effect of the multiple small-angle scattering is assumed to be negligible at distances of order λ_u but can be substantial when accumulated over many undulator periods.

For further calculations it is convenient to rewrite Eqs. (8) and (9) in a shorter notation (we omit the index 0 of the transverse velocity because $\mathbf{v}_t$ is now a function of z),

$$\frac{du}{dz} = \omega\beta J_0\left[\frac{\omega a_u v_t(z)}{\gamma_i\Omega}\right]\sin\left[\Phi - \frac{\omega a_u v_y(z)}{\gamma_i\Omega}\right] , \tag{12}$$

$$\frac{d\Phi}{dz} = \frac{\omega}{2}[\mu - bu(z) + v_t^2(z)] , \tag{13}$$

where $u=(\gamma/\gamma_i)^2-1$ is a new independent variable, γ_i is the particle initial Lorentz-factor, $\beta=2a_s a_u/\gamma_i^2 \ll 1$ is a new small parameter, and b and μ are constants defined as

$$b = \frac{1+a_u^2}{\gamma_i^2} , \tag{14}$$

$$\mu = b - \chi'(\omega) - \frac{2\Omega}{\omega} . \tag{15}$$

The initial condition for the new variable u is $u(z=0)=0$, and in the small-signal regime u is assumed to be small: $|u| \ll 1$. With the help of the energy conservation law, the small-signal gain per pass may be expressed in terms of u as

$$G = -\frac{2\pi e^2 n_b \gamma_i}{m\omega^2 a_s^2}\langle u(L)\rangle_\Phi , \tag{16}$$

where e is the electron charge, n_b is the beam density, and L is the length of the undulator. The brackets indicate averaging over the initial phase Φ_0 from 0 to 2π.

Integrating now Eqs. (12) and (13) over z from 0 to L, expanding them in β up to the second order and averaging over Φ_0, one has the following expression for the average energy transfer from the particle to the electromagnetic wave in a distance L:

$$\begin{aligned}\langle u(L)\rangle_\Phi = \frac{b\beta^2\omega^3}{4}\int_0^L dz_1 J_0\left[\frac{\omega a_u v_t(z_1)}{\gamma_i\Omega}\right] \\ \times\int_0^{z_1} dz_2 (z_1-z_2) J_0\left[\frac{\omega a_u v_t(z_2)}{\gamma_i\Omega}\right] \\ \times\sin\left[\frac{\omega a_u}{\gamma_i\Omega}[v_y(z_1)-v_y(z_2)] \right. \\ \left. +\frac{\omega}{2}\int_{z_2}^{z_1} dz_3[\mu + v_t^2(z_3)]\right] .\end{aligned} \tag{17}$$

With the help of Eq. (17) one could find the energy transfer from any given particle trajectory, that is, for any given dependence $\mathbf{v}_t(z)$, $0<z<L$. But in a scattering medium the consideration of a trajectory of an individual electron has not much physical sense. To obtain a meaningful result, we should average the quantity under consideration over all possible trajectories. Equation (17) has

an advantage for this task because it is written in the form of a two-point correlation function of an electron trajectory. We may, therefore, apply a special technique developed by Migdal [14] for averaging such functions over trajectories.

Equation (17) contains the two following kinds of parameters of a trajectory: first, the transverse velocity $\mathbf{v}_t$ at different distances z, and second, a special combination of the transverse velocities, which we shall denote as ξ,

$$\xi(z,z') \equiv \int_z^{z'} dx\, v_t^2(x) \ . \tag{18}$$

The $\omega\xi/2$ term in the argument of the sine in Eq. (17) carries information about coherence between different parts of the electron trajectory and, therefore, needs an accurate treatment.

Let $w_1(\mathbf{v}_t,z)$ be the probability for a particle to have the transverse velocity $\mathbf{v}_t$ at the distance z, and $w_2(\xi,\mathbf{v}_t',z'|\mathbf{v}_t,z)$ be the probability to have the "coordinate" ξ and the transverse velocity $\mathbf{v}_t'$ at the distance z', provided that at the distance z this "coordinate" and velocity were equal to 0 and $\mathbf{v}_t$, respectively. Averaging of Eq. (17) over all possible trajectories then means

$$\langle\langle u(L)\rangle_\Phi\rangle_{\text{traject}} = -\frac{b\beta^2\omega^3}{4}\,\text{Im}\int_0^L dz_1 \int_0^{z_1} dz_2 (z_1-z_2)\exp\left[-i\frac{\omega\mu}{2}(z_1-z_2)\right]$$
$$\times \int d^2v_t\, w_1(\mathbf{v}_t,z_2)\int_{-\infty}^{\infty} d\xi \int d^2v_t'\, w_2(\xi,\mathbf{v}_t',z_1|\mathbf{v}_t,z_2)$$
$$\times J_0\left[\frac{\omega a_u v_t}{\gamma_i\Omega}\right] J_0\left[\frac{\omega a_u v_t'}{\gamma_i\Omega}\right]\exp\left[-i\frac{\omega a_u}{\gamma_i\Omega}(v_y'-v_y)-i\frac{\omega}{2}\xi\right] \ . \tag{19}$$

The transverse velocity distribution w_1 is well known in the theory of multiple scattering [15]. It is a Gaussian distribution, the width of which grows linearly with the depth of a particle penetration into a medium,

$$w_1(\mathbf{v}_t,z) = \frac{1}{\pi(4qz+\theta_0^2)}\exp\left[-\frac{v_t^2}{4qz+\theta_0^2}\right] , \tag{20}$$

where θ_0 is the angular spread of the beam at the entrance of the undulator, $q \equiv \langle\theta_S^2\rangle/4$ is the only parameter describing the multiple scattering, and $\langle\theta_S^2\rangle$ is the mean square of the scattering angle of the particle per unit path. The latter is defined as

$$\langle\theta_S^2\rangle = Nv\int d\theta\,\theta^2\frac{d\sigma}{d\theta} \ , \tag{21}$$

where N is the density of the medium, $d\sigma/d\theta$ is the elastic cross section, and θ is the angle between the initial and the final particle momenta. For applications, it is convenient to present the parameter$q$ as

$$q = \frac{N}{N_{\text{STP}}}\frac{1}{\gamma_i^2 R} \ , \tag{22}$$

where R is a characteristic length (see Table I).

As for the correlation probability function w_2, it is known to satisfy a kinetic equation that can be reduced to the Fokker-Planck equation [15]. Because of space-time uniformity, w_2 obviously depends only on the difference between z_1 and z_2; in the following we shall denote it as τ:

$$\tau \equiv z_1 - z_2 \ .$$

In the small-angle approximation, one thus obtains [14]

$$\frac{\partial w_2}{\partial\tau} + (v_t')^2\frac{\partial w_2}{\partial\xi} = q\Delta_{v_t'}w_2 \ , \tag{23}$$

where

$$\Delta_{v_t} = \left[\frac{\partial^2}{\partial v_x^2}+\frac{\partial^2}{\partial v_y^2}\right]$$

is the Laplace operator in the transverse velocity space. Equation (23) is to be solved under the following initial condition:

$$w_2(\tau=0) = \delta(\xi)\delta(\mathbf{v}_t'-\mathbf{v}_t) \ . \tag{24}$$

It is convenient to define a new function

$$F(\mathbf{v}_t,\mathbf{v}_t',\tau) \equiv \int_{-\infty}^{\infty} d\xi\, w_2(\xi,\mathbf{v}_t',\tau|\mathbf{v}_t)\exp\left[-i\frac{\omega}{2}\xi\right] \ . \tag{25}$$

Combining Eqs. (23)–(25), one has

$$\frac{\partial F}{\partial\tau} + i\frac{\omega}{2}(v_t')^2 F = q\Delta_{v_t'}F \tag{26}$$

with the initial condition

$$F(\tau=0) = \delta(\mathbf{v}_t'-\mathbf{v}_t) \ . \tag{27}$$

The solution of Eqs. (26) and (27) can be found as

$$F(\mathbf{v}_t,\mathbf{v}_t',\tau) = \frac{1}{\pi\sinh(\sqrt{2i\omega q}\,\tau)}\left[\frac{i\omega}{8q}\right]^{1/2}$$
$$\times\exp\left[\left[\frac{i\omega}{8q}\right]^{1/2}\left[\frac{2\mathbf{v}_t\cdot\mathbf{v}_t'}{\sinh(\sqrt{2i\omega q}\,\tau)}-[v_t^2+(v_t')^2]\coth(\sqrt{2i\omega q}\,\tau)\right]\right] \ . \tag{28}$$

Substituting the above expressions for w_1 and F into Eq. (19), one has

$$\langle\langle u(L)\rangle_{\Phi}\rangle_{\text{traject}} = -\frac{b\beta^2\omega^3}{4\pi^2}\text{Im}\int_0^L dz\int_0^{L-z}d\tau\left[\frac{i\omega}{8q}\right]^{1/2}\frac{\tau}{\sinh(\sqrt{2i\omega q}\,\tau)}\exp\left[-i\frac{\omega\mu\tau}{2}\right]$$
$$\times\int d^2v_t\frac{1}{4qz+\theta_0^2}\exp\left[-\frac{v_t^2}{4qz+\theta_0^2}\right]J_0\left[\frac{\omega a_u v_t}{\gamma_i\Omega}\right]\int d^2v_t'\exp\left[-i\frac{\omega a_u}{\gamma_i\Omega}(v_y'-v_y)\right]$$
$$\times J_0\left[\frac{\omega a_u v_t'}{\gamma_i\Omega}\right]\exp\left[\left[\frac{i\omega}{8q}\right]^{1/2}\left[\frac{2\mathbf{v}_t\cdot\mathbf{v}_t'}{\sinh(\sqrt{2i\omega q}\,\tau)}-[v_t^2+(v_t')^2]\coth(\sqrt{2i\omega q}\,\tau)\right]\right]. \quad (29)$$

This is the expression for the energy transfer that takes into account phase "jitter" and coherence loss due to multiple scattering.

In the most general case, one should average the above expression over a distribution of the initial energy of the particles in the beam. For the Gaussian form

$$w(\gamma_i)=\frac{1}{\sqrt{2\pi}\gamma_0\sigma_\gamma}\exp\left[-\frac{(\gamma_i-\gamma_0)^2}{2\gamma_0^2\sigma_\gamma^2}\right] \quad (30)$$

this averaging involves a simple change in Eq. (29)

$$\exp\left[-i\frac{\omega\mu\tau}{2}\right]\rightarrow\exp\left[-i\frac{\omega\mu_0\tau}{2}-\frac{b_0^2\omega^2\sigma_\gamma^2\tau^2}{2}\right], \quad (31)$$

where b_0 and μ_0 are defined as

$$b_0=\frac{1+a_u^2}{\gamma_0^2}, \quad (32)$$

$$\mu_0=b_0-\chi'(\omega)-\frac{2\Omega}{\omega}. \quad (33)$$

The relative energy spread in the beam σ_γ is assumed to be small, $\sigma_\gamma\ll 1$, therefore, in all other terms of Eq. (29) the particle energy γ_i may be taken equal to the average energy of the beam γ_0.

The six-dimensional integral in Eq. (29) can be reduced to a four-dimensional one (see Appendix B). Taking into account Eqs. (31) and (16) as well, we arrive at

$$G=\frac{2e^2n_ba_u^2(1+a_u^2)}{\pi m\omega^{1/2}q^{3/2}\gamma_0^5}\text{Im}\int_{T_0}^{T_0+L\sqrt{\omega q}}dT\int_0^{T_0+L\sqrt{\omega q}-T}dt\,tD(T,t)\exp\left[-i\frac{\mu_0 t}{2}\left[\frac{\omega}{q}\right]^{1/2}-\frac{b_0^2\omega\sigma_\gamma^2t^2}{2q}\right]$$
$$\times\int_0^\pi d\phi\int_0^\pi d\psi\exp\{-QTD(T,t)[(2-\cos\phi-\cos\psi)\cosh(t\sqrt{2i}\,)-(1-\cos\phi)(1-\cos\psi)]\}$$
$$\times\exp\left[-\frac{QD(T,t)}{\sqrt{2i}}(1-\cos\phi)\sinh(t/\sqrt{2i}\,)\right]\cosh[QTD(T,t)\sin\phi\sin\psi], \quad (34)$$

where

$$D(T,t)=\frac{1}{\cosh(t\sqrt{2i}\,)+T\sqrt{2i}\sinh(t/\sqrt{2i}\,)}$$

and

$$T_0=\frac{\theta_0^2}{4}\left[\frac{\omega}{q}\right]^{1/2}. \quad (35)$$

The dimensionless parameter

$$Q\equiv\frac{2a_u^2\omega^{3/2}q^{1/2}}{\Omega^2\gamma_0^2} \quad (36)$$

characterizes the influence of the "phase jitter" for a helical GFEL.

Equation (34) is our final result for the small-signal gain per pass in a GFEL. The only step to be made is to include the absorption of light in the medium (in fact, below the resonant atomic frequency there is no real absorption, only scattering, but in our considerations we may ignore the difference). The effective gain is then the difference between the amplification and the absorption of the wave,

$$G_{\text{eff}}=G-2Lh(\omega), \quad (37)$$

where $2L$ is two times the undulator length, i.e., the minimal length of the roundtrip path, and h is the extinction coefficient. For gaseous media the extinction coefficient is [13]

$$h=\frac{2\omega^4}{3\pi N}(n-1)^2. \quad (38)$$

Because of the sharp ω dependence of the refractive index n [see Eqs. (3) and (4)], absorption will be important only at frequencies close to the resonant frequencies of the gas molecules.

IV. NUMERICAL RESULTS AND DISCUSSION

We have derived a rather long and complicated expression for the gain in a GFEL, which can be studied only numerically. But before turning to numerical calcula-

tions, it is instructive to consider some simple limiting cases.

Let us first separate the influence of the "phase jitter" and of the coherence loss. The "jitter" is negligible if the above parameter Q [see Eq. (36)] is small (one may formally consider this as the limiting case of a small undulator parameter, $a_u \to 0$). The influence of the coherence loss remains unchanged in this limit. Putting $Q \to 0$, one obtains from Eq. (34)

$$\int_0^{\pi} d\phi \int_0^{\pi} d\psi \cdots \to \pi^2 ,$$

and, therefore,

$$G = \frac{2\pi e^2 n_b a_u^2 (1+a_u^2)}{m\omega^{1/2} q^{3/2} \gamma_0^5} \mathrm{Im} \int_0^{L/\sqrt{\omega q}} dt \frac{t}{\sqrt{2i}\sinh(t\sqrt{2i})} \times \exp\left[-i\frac{\mu_0 t}{2}\left(\frac{\omega}{q}\right)^{1/2} - \frac{b_0^2 \omega \sigma_\gamma^2 t^2}{2q} \right] \times \ln\left[1 + \frac{\sqrt{2i}\,(L\sqrt{\omega q} - t)\tanh(t\sqrt{2i})}{1+\sqrt{2i}\,T_0 \tanh(t\sqrt{2i})} \right] . \quad (39)$$

One can see from Eq. (39) that the initial angular spread of the beam (which is represented by T_0) is not equivalent to the influence of multiple scattering (which is proportional to q). It means, generally speaking, that the latter cannot be represented merely as a growth of the beam emittance, as was assumed in [8]. The difference comes from taking into account the possibility of coherence loss between different parts of the particle trajectory.

As an illustration, the ratio R of the exact result [Eq. (39)] and a "naive" result, which assumes usage of an ordinary small-signal gain expression for a vacuum FEL with distance-dependent [corresponding to the multiple scattering theory, see Eqs. (20)–(22)] beam emittance, is shown in Fig. 1. The ratio is presented as a function of the undulator length L measured in units of some "coherence scale" L_q which is defined as

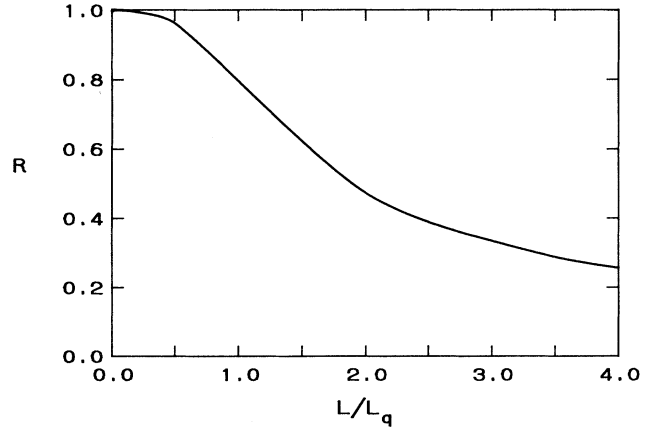

FIG. 1. The ratio of the small-signal gain calculated from Eq. (39) and from a simplified approach, assuming usage of an ordinary small-signal gain expression for a vacuum FEL with a predescribed distance-dependent beam emittance, as a function of the dimensionless undulator length L/L_q [Eq. (40)].

$$L_q \equiv 4/\sqrt{\omega q} . \quad (40)$$

One can see that the "naive" approach is reasonably correct at $L < L_q$ but may strongly overestimate the small-signal gain as the undulator length becomes larger than L_q. To be specific, let us take $\gamma_0 = 100$ and consider a gas pressure $P \sim 0.1$ atm. In the infrared range, the corresponding scale is then rather long: $L_q \sim (3-5)$ meters for $\lambda = (2-4)$ μm. But it becomes considerably shorter as one approaches the VUV region. For the wavelengths nearby the hydrogen cutoff wavelength ($\lambda = 121.6$ nm) the scale L_q is about 70 cm. For the helium cutoff wavelength ($\lambda = 58.4$ nm) it is even shorter: $L_q \sim 40$ cm. The influence of the coherence loss thus becomes increasingly important as the wavelength decreases; consequently, the assumption of an increase in emittance becomes less valid.

The transition to the case of a vacuum FEL can be traced as well. This corresponds to the limit $q \to 0$. The upper limit of the integral in Eq. (39) then becomes small, $L\sqrt{\omega q} \ll 1$. One may, therefore, expand hyperbolic and logarithmic functions in the integrand into series in t and take lowest-order terms. Introducing a new variable $x \equiv t/\sqrt{\omega q}$ and using Eq. (35), one has

$$G = \frac{2\pi e^2 n_b \omega a_u^2 (1+a_u^2)}{m\gamma_0^5} \mathrm{Im} \int_0^t dx \frac{x(L-x)}{(1+i\omega\theta_0^2 x/2)} \times \exp\left[-i\frac{\omega}{2}\left(\frac{1+a_u^2}{\gamma_0^2} - \frac{2\Omega}{\omega} - \chi' \right) x - \frac{b_0^2 \omega^2 \sigma_\gamma^2 x^2}{2} \right] . \quad (41)$$

For generality, we keep a nonzero refractive term χ', as if refraction could be introduced without scattering; in the limit $\chi' \to 0$ the above expression describes the small-signal gain per pass of a vacuum FEL with finite angular and energy spread of the electron beam. In the limit $\sigma_\gamma \to 0$ and $\theta_0^2 \to 0$ we arrive at the expression

$$G = \frac{\pi e^2 n_b a_u^2 (1+a_u^2) \omega L^3}{2m\gamma_0^5} \times \frac{d}{d\theta}\left[\frac{\sin^2\theta}{\theta^2} \right]_{\theta = \omega L/4[(1+a_u^2)/\gamma_0^2 - 2\Omega/\omega - \chi']} , \quad (42)$$

which is identical to the well-known formula for the vacuum case [16] if $\chi' = 0$. Our result thus correctly reproduces expressions for ordinary FEL's.

To illustrate the above statement and to check our numerical scheme, we made computations of the gain at different energies of the electron beam with the help of Eq. (34) and compared them with the analytical formula Eq. (42). The generated wavelength was taken to be 130 nm; the value of χ' was chosen such that exact synchronism corresponded to $\gamma_0 = 100$. The following undulator parameters are used in our numerical calculations throughout the paper: $\lambda_u = 2$ cm, $B_0 = 5$ kG, $a_u \approx 1$. The results (in arbitrary units) are presented in Fig. 2; the dotted line is obtained from Eq. (34) and the circles from Eq. (42). One can see the excellent consistency of the two sets of data.

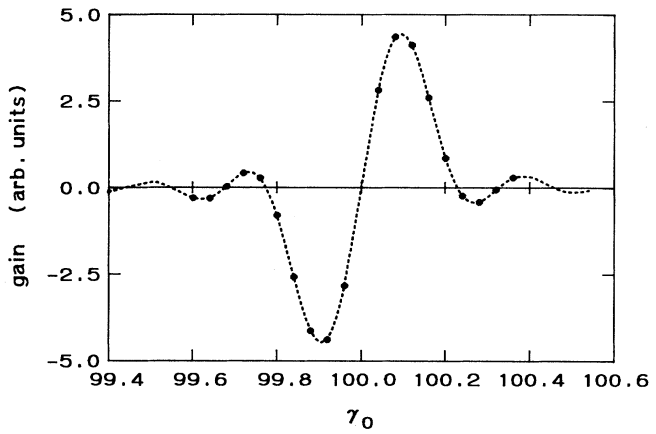

FIG. 2. The small-signal gain per pass as a function of the particle energy for an idealized case wherein the multiple scattering, as well as angular spread and energy spread of the beam, are neglected. The dotted line is the result of direct numerical calculations from Eq. (34), circles are the analytical expression for the limiting case of a vacuum FEL with refraction [Eq. (42)]. The undulator parameters are $\lambda_u=2$ cm, $B_0=5$ kG, the generated wavelength is $\lambda=130$ nm.

The influence of different effects on the small-signal gain is illustrated in Fig. 3. For the same parameters as in Fig. 2, we calculate the gain: (i) without energy spread and multiple scattering, (ii) taking into account only the energy spread with $\sigma_\gamma=1\times10^{-3}$, and (iii) with both multiple scattering and an energy spread of $\sigma_\gamma=1\times10^{-3}$ taken into account. The gas inside the cavity is hydrogen. One can see from Fig. 3 that even as small a relative energy spread as 10^{-3} noticeably reduces the gain in the short wavelength region (dashed line). The addition of multiple scattering not only further reduces the gain but

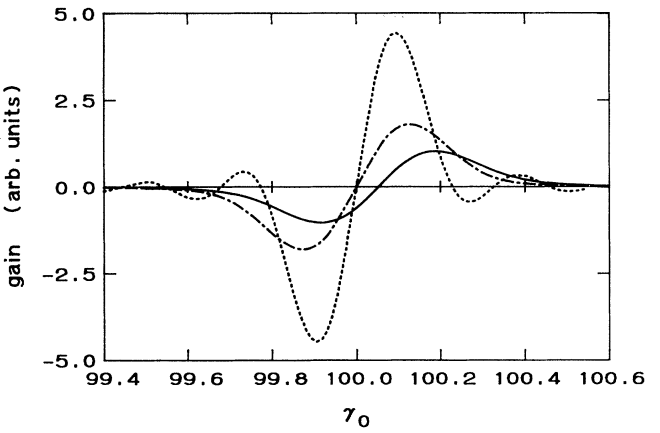

FIG. 3. The influence of different effects on the gain curve of a GFEL at short wavelength. Dotted line, no multiple scattering, no energy spread (same as for Fig. 2); dashed line, no multiple scattering, the relative energy spread is $\sigma_\gamma=1\times10^{-3}$; solid line, the same energy spread together with multiple scattering. The undulator parameters are the same as in Fig. 2. The gas inside the cavity is hydrogen, the pressure is adjusted for generation at 130 nm and equals to ~0.08 atm.

also makes the gain curve asymmetric (solid line).

We now turn to the magnitude of the GFEL gain and the beam parameters necessary for lasing in the ultraviolet. For realistic estimates, it should be noted that the parameters appearing in Eq. (34) are not independent. Because of 3D effects, the beam density n_b is in fact a function of the longitudinal coordinate z and strongly depends on the beam waist radius r_0. In turn, the latter, as well as the initial angular spread θ_0, is connected to the undulator length L. To incorporate all this with the 1D expressions obtained above, the following procedure was adopted.

We keep the four most important beam parameters fixed: the total current of the beam I, the average energy γ_0, the energy spread σ_γ and the normalized emittance $\epsilon_N\equiv\pi\gamma_0 r_0\theta_0$. Then n_b is estimated as

$$n_b=\frac{I}{eS_{\text{eff}}}\ , \tag{43}$$

where S_{eff} is some effective (averaged over the longitudinal coordinate) cross-section area of the beam inside the cavity. The beam is always focused onto the undulator axis to reach a high-current density, but it cannot be focused too much because it has to match the optical mode along the whole undulator length. If the electron beam waist is situated nearly in the middle of the interaction area and r_0 is the waist radius, then the beam radius at the ends of the undulator can be estimated as

$$r\left[\frac{L}{2}\right]\approx r_0+\frac{L}{2}\theta_0=r_0+\frac{L\epsilon_N}{2\pi\gamma_0 r_0}\ . \tag{44}$$

Minimizing Eq. (44) with respect to r_0, one has

$$r_0\approx\sqrt{L\epsilon_N/2\pi\gamma_0} \tag{45}$$

for the waist radius at which the optical mode matches the beam in an optimal way. The radius of the beam at the ends of the undulator is then two times larger than in the center. The corresponding initial angular spread is, in this case,

$$\theta_0=\frac{\epsilon_N}{\pi\gamma_0 r_0}\approx\left[\frac{2\epsilon_N}{\pi L\gamma_0}\right]^{1/2}\ . \tag{46}$$

In addition to its intrinsic size, there is also beam broadening due to multiple scattering. At a distance of about one half of the undulator length, the beam radius associated with the scattering is roughly [15]

$$r_{\text{scat}}\approx\left[\frac{qL^3}{6}\right]^{1/2}\ . \tag{47}$$

The minimal cross-section area of the beam inside the cavity may then be estimated as $S_{\min}\approx\pi(r_0^2+r_{\text{scat}}^2)$. In the following we shall assume S_{eff} to be two times $S_{\min}$:

$$S_{\text{eff}}=2\pi(r_0^2+r_{\text{scat}}^2)\ , \tag{48}$$

where the coefficient 2 gives a reasonable estimate of the averaging over the longitudinal coordinate; any more realistic z dependence of the beam radius would lead to a

similar result. Equations (43)–(46) now express all necessary quantities in the four beam parameters and the undulator length L.

We do not include slippage effects into our considerations, assuming the electron bunch to be sufficiently long. It is known, however, that slippage is very important near atomic resonances because of strong group velocity dispersion. One can find a detailed discussion of these effects in [9].

A GFEL is thought to be easily tuned with the help of changing the gas pressure inside the cavity. In a sense, this is similar to the tuning of an ordinary FEL with the help of changing of the beam energy. For any given wavelength there is then a certain gas density at which the gain has its maximum. A more surprising feature of the GFEL is that there exists an optimal undulator length as well. This is because of the scattering of particles inside the cavity. At relatively short distances, the gain is proportional to the undulator length as in ordinary FEL's. But when the undulator becomes too long, the "damage" to the beam outweighs all other effects, the beam cross section becomes too large [see Eqs. (47) and (48)] and the gain starts to decrease as the undulator length increases. A typical dependence of the gain per pass on the undulator length is shown in Fig. 4.

Taking into account the above statements, we included an optimization procedure into our computation. Namely, for a fixed beam parameter, the gas density and the undulator length were varied until the maximum of the gain was reached. One thus obtains three curves simultaneously: the "resonant" pressure of the gas, the optimal undulator length and the gain as a function of the output frequency. Some of these curves are presented in the following figures.

Figure 5 shows a typical tuning curve of a GFEL: the gas density (or pressure, if its temperature is kept fixed) as a function of the energy of the photons emitted. The gas inside the cavity is hydrogen, the beam energy is 50 MeV, the undulator parameters coincide with those for Fig. 2. The curve is double valued: two different frequencies

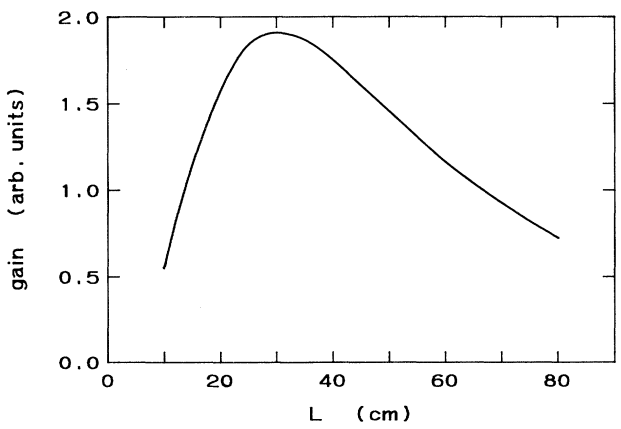

FIG. 4. Typical dependence of the gain per pass on the undulator length. The wavelength is $\lambda = 130$ nm, the gas inside the cavity is hydrogen at 0.08 atm, the beam energy is 50 MeV. The undulator parameters are the same as for Fig. 2.

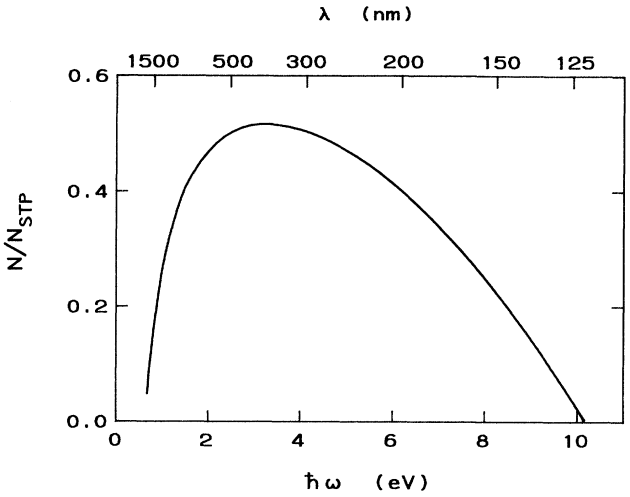

FIG. 5. The tuning curve of a GFEL: the gas density (relative to its density at STP) as a function of the energy of the photons emitted. The gas inside the cavity is hydrogen, the beam energy is 50 MeV, the period of the undulator is 2 cm, magnetic field on the axis is 5 kG.

may be generated at the same pressure [7], as a result of the ω dependence of the refractive index n [see Eqs. (3) and (4)]. One sees from the figure that tuning over the whole interval from the infrared to the ultraviolet is possible with the introduction of less than 1 atm of hydrogen into the cavity. Unfortunately, multiple scattering strongly damages the beam at pressures higher than approximately 0.1 atm (see below), therefore, real tuning is only possible nearby the left and the right ends of the curve.

The next figure illustrates the influence of the beam parameters. The gain per unit beam current G/I is shown as a function of the photon energy for different normalized emittances and energy spreads of the beam. There are two different sets of data in this figure: three curves for hydrogen filling in the range 1–10 eV for a beam energy of 50 MeV and two curves for helium filling in the range 3–21 eV for beam energies of 50 and 80 MeV. One can clearly see the extremely strong dependence of the gain on the beam quality. For hydrogen filling, a reduction of the normalized emittance from 50π to 5π mm mrad leads to a gain enhancement of more than 20 times at photon energies $\hbar\omega \sim (9-10)$ eV. A reduction of the energy spread from 3×10^{-3} to 1×10^{-3} leads to further improvement of the gain by nearly one order of magnitude. For the helium curves, the gain appears to be much lower at a beam energy of 50 MeV even for the best beam quality ($\epsilon_N = 5\pi$ mm mrad, $\sigma_\gamma = 1\times10^{-3}$). This is due to the fact that helium requires pressure four times higher to reach the same refractive index; respectively, multiple scattering strongly reduces the small-signal gain. To obtain a higher gain, one needs to increase the beam energy. For this reason, the calculations for helium filling were performed also at a beam energy of 80 MeV for the same beam quality. Nearly one order of magnitude enhancement of the gain can be seen in the picture.

One should also note a common feature of the curves in Fig. 6: they all have a broad and deep plateau in the central part with sharp maxima at the ends. This is because of the ω dependence of the gas pressure. The central parts of the curves correspond to a rather high density of the gas inside the cavity (see Fig. 5), therefore, the gain is strongly reduced with multiple scattering.

To obtain insight into the beam current necessary for lasing in the ultraviolet, it is convenient to represent the same data in a different way. Namely, let us define I_η as the current at which the maximum of the effective gain G_{eff} [see Eq. (37)] equals to η. Then $I_{\eta 0}(\omega)$ is the starting current for laser oscillation at the frequency ω if η_0 is the corresponding wave attenuation per roundtrip in the optical cavity. Somewhat arbitrarily, we choose $\eta_0=0.2$; this gives a reasonable estimate of the losses for photon energies below 10 eV, where high-finesse cavities are available, and may be too optimistic in the range 10–20 eV. The corresponding starting current $I_{0.2}$ as a function of the photon energy ω is shown in Fig. 7.

We present again two sets of curves corresponding to hydrogen and helium filling of the cavity. Sharp minima nearby the cutoff frequency are the result of light absorption [see Eqs. (37) and (38)]. For the same beam parameters, the starting current for hydrogen appears to be considerably lower than for helium. With hydrogen filling, the starting current at a photon energy 9–10 eV is seen to drop below 10 A for beam parameters accessible for modern linacs with photoinjectors (see e.g., [17]): $\gamma_0=100$, $\epsilon_N=5\pi$ mm mrad, $\sigma_\gamma=1\times10^{-3}$. Hence, hydrogen filling appears to be a promising avenue for lasing in the VUV region.

For higher photon energies (between 10 and 20 eV) the situation is less optimistic. Even for such low intracavity losses as 0.2 and a beam energy of 80 MeV, the starting current remains above 30–50 A. But a more realistic estimate of the cavity finesse in this range of wavelengths would give a 2–3 times higher value for the starting current. Such a current can already lead to a significant degradation of the refractive index of the medium during one macropulse, unless special measures, such as addition of a small fraction of a dopant gas [18], are taken. GFEL operation in the range 10–20 eV thus seems much more difficult.

The typical dependence of the optimal undulator length on the photon energy is shown in Fig. 8. A GFEL operating in the VUV region appears to be a compact device: the optimal undulator design has only 10–30

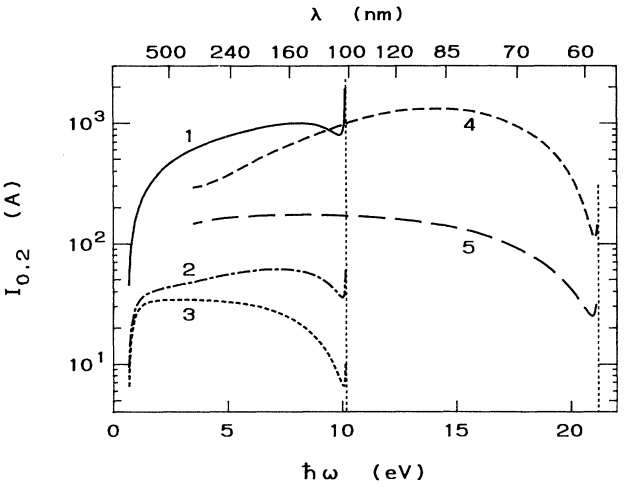

FIG. 7. The starting current $I_{0.2}$, required to obtain laser oscillation at a roundtrip loss of 20%, for the same beam and undulator parameters as for Fig. 6. See the caption of Fig. 6 for further details.

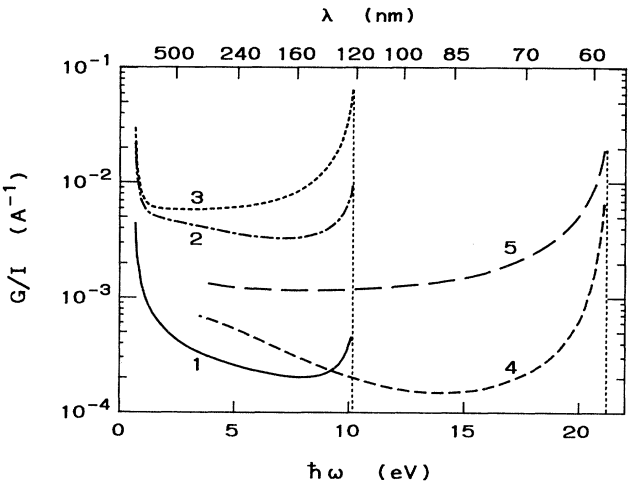

FIG. 6. The gain per unit beam current G/I as a function of the photon energy for different beam parameters. The curves 1–3 pertain to hydrogen filling of the optical cavity: (1) $\gamma_0=100$, $\sigma_\gamma=3\times10^{-3}$, $\epsilon_N=50\pi$ mm mrad; 2—$\gamma_0=100$, $\sigma_\gamma=3\times10^{-3}$, $\epsilon_N=5\pi$ mm mrad; 3—$\gamma_0=100$, $\sigma_\gamma=1\times10^{-3}$, $\epsilon_N=5\pi$ mm mrad. The curves 4 and 5 pertain to helium filling: 4—$\gamma_0=100$, $\sigma_\gamma=1\times10^{-3}$, $\epsilon_N=5\pi$ mm mrad; 5—$\gamma_0=160$, $\sigma_\gamma=1\times10^{-3}$, $\epsilon_N=5\pi$ mm mrad. The undulator parameters are $\lambda_u=2$ cm, $B_0=5$ kG.

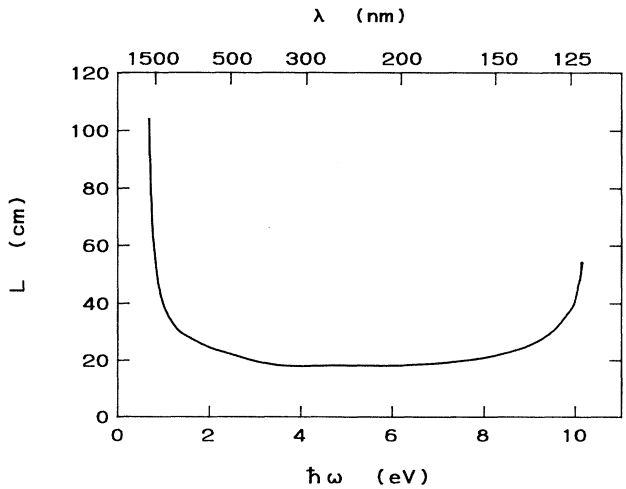

FIG. 8. The optimal undulator length as a function of the energy of photons. The beam energy is 50 MeV, the gas inside the cavity is hydrogen, the undulator parameters are the same as for Fig. 6.

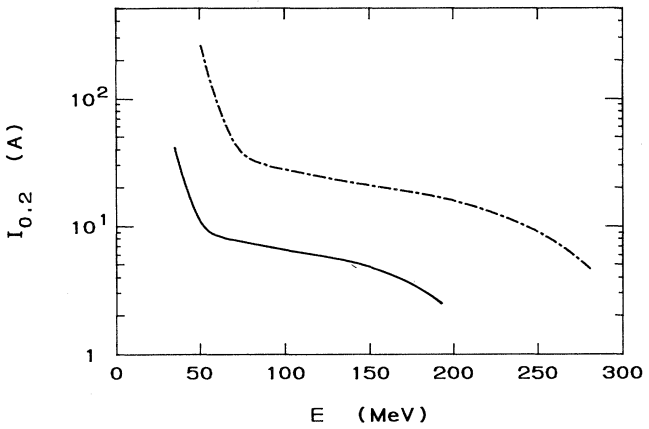

FIG. 9. The starting current $I_{0.2}$ as a function of the beam energy. The upper curve, helium, $\lambda=61$ nm; the lower curve, hydrogen, $\lambda=130$ nm. The undulator parameters are $\lambda_u=2$ cm, $B_0=5$ kG.

periods and a total length of 20–100 cm. The corresponding intracavity electron beam radius is then very small, of order 100–200 μm. When the beam energy γ_0 is increased, the optimal undulator length scales approximately as γ_0^2.

An attractive feature of a GFEL is the possibility to provide ultraviolet radiation with a relatively low-current and low-energy accelerator; such a machine is relatively inexpensive. To study GFEL prospects in this respect, we calculated the starting current $I_{0.2}$ for different beam energies. The undulator parameters were the same as for Fig. 2: $\lambda_u=2$ cm, $B_0=5$ kG. The results are shown in Fig. 9. One can see the rather weak dependence of $I_{0.2}$ on the beam energy above some characteristic energy and a sharp increase below it. This is mainly a result of the "phase jitter." Its influence is noticeable if the corresponding parameter Q [see Eq. (36)] is larger than unity, $Q>1$. In turn, Q strongly depends on γ_0; above a certain beam energy the "jitter" becomes, therefore, negligible. The typical energy range is above 50 MeV for hydrogen filling and above 80 MeV for helium filling.

V. CONCLUSIONS

We have considered the influence of multiple scattering on the small-signal gain in a gas-loaded FEL. The influence was shown to be increasingly important in the short wavelength region. Two new effects were considered, as compared to ordinary helical FEL's: the phase "jitter" of a particle over one undulator period and the coherence loss between different parts of the particle trajectory. Both lead to a significant gain reduction in the short wavelength region. Analytical forms accounting for the above effects were obtained in a one-dimensional approximation.

Numerical calculations were made to obtain insight into the beam and undulator parameters necessary for lasing in the ultraviolet. The hydrogen-filled GFEL's were shown to have good prospects for this at today's technological level. To suit this task in the range of wavelength 125–140 nm, an electron beam should have an energy above 50 MeV and a good quality: a normalized emittance of order 5π mm mrad and an energy spread below 10^{-3}. All these parameters are achievable with modern linacs and photoinjectors.

The undulator length was shown to have an optimum that is connected to the influence of multiple scattering on the radius of the electron beam as it passes through the gas inside optical cavity. The optimal design for wavelengths 125–140 nm involves 10–30 periods and a total length of 20–100 cm; a GFEL operating in the VUV region thus appears to be a compact device. One can reach a gross small-signal gain of 20% with only 10 A of electron beam current.

The numerical scheme adopted in our calculations is based on a one-dimensional approach and does not include many additional effects such as, for instance, beam scattering in the input foil separating the accelerator vacuum and the undulator area, group velocity dispersion, the transverse structure of the optical mode, etc. On the other hand, it takes into account the most important features of GFEL and may serve as a good basis for further considerations.

ACKNOWLEDGMENTS

The authors are grateful to Professor R. H. Pantell of Stanford University for his useful comments. This work was performed as part of the research programme of the Stichting voor Fundamenteel Onderzoek der Materie (FOM) and was supported by the Nederlandse Organisatie voor Wetenschappelijk Onderzoek (NWO).

APPENDIX A: AVERAGING OF THE PENDULUM EQUATIONS OVER ONE UNDULATOR PERIOD

In order to simplify the equations, one should first divide the variables ϵ and Φ into "slow" and "fast" parts, $\epsilon\rightarrow\epsilon+\tilde{\epsilon}$, $\Phi\rightarrow\Phi+\tilde{\Phi}$, where $\tilde{\epsilon}$ and $\tilde{\Phi}$ represent now "fast" motions with typical frequency Ω, which have to be averaged out to obtain the equations of motion for the "slow" variables ϵ and Φ. The fast energy variation $\tilde{\epsilon}$ is seen from Eq. (1) to be proportional to the small parameter a_s. In the lowest nonvanishing order we may, therefore, neglect $\tilde{\epsilon}$ terms and consider the energy ϵ as a constant when averaging the equations of motion over the "fast" time scale.

The quantity of interest is then the phase Φ. From Eq. (7) one can find an approximate solution for $\tilde{\Phi}$ within one undulator period,

$$\tilde{\Phi}(\tilde{z})=-\frac{\omega m a_u}{\epsilon\Omega}(v_{0x}\sin\Omega\tilde{z}-v_{0y}\cos\Omega\tilde{z}+v_{0y}) , \qquad \text{(A1)}$$

where $\tilde{z}\equiv z-N\lambda_u$ is the longitudinal coordinate of the particle, taken from the beginning of an undulator period, $0<\tilde{z}<\lambda_u$.

Equation (7) is linear in $\tilde{\Phi}$; the averaging is, therefore, trivial and leads simply to cancellation of the terms containing $\sin\Omega z$ and $\cos\Omega z$ [see Eq. (9)]. As for Eq. (1), it is essentially nonlinear in $\tilde{\Phi}$. The averaging over one undulator period then gives

$$\sin\Phi \to \frac{1}{\lambda_u}\int_0^{\lambda_u} d\tilde{z}\,\sin[\Phi+\tilde{\Phi}(\tilde{z})] = \frac{1}{\lambda_u}\int_0^{\lambda_u} d\tilde{z}\,\sin\left[\Phi-\frac{\omega m a_u}{\epsilon\Omega}(v_{0x}\sin\Omega\tilde{z}-v_{0y}\cos\Omega\tilde{z}+v_{0y})\right]$$

$$=\frac{1}{2\pi}\int_0^{2\pi} d\xi\,\sin\left[\Phi-\frac{\omega m a_u}{\epsilon\Omega}v_{0y}\right]\cos\left[\frac{\omega m a_u}{\epsilon\Omega}(v_{0x}\sin\xi-v_{0y}\cos\xi)\right]$$

$$-\frac{1}{2\pi}\int_0^{2\pi} d\xi\,\cos\left[\Phi-\frac{\omega m a_u}{\epsilon\Omega}v_{0y}\right]\sin\left[\frac{\omega m a_u}{\epsilon\Omega}(v_{0x}\sin\xi-v_{0y}\cos\xi)\right].$$

The latter of the above integrals cancels because of the antisymmetric integrand, while the former leads to the final expression,

$$\sin\Phi \to \frac{1}{\pi}\sin\left[\Phi-\frac{\omega m a_u}{\epsilon\Omega}v_{0y}\right]\int_0^{\pi} d\xi'\cos\left[\frac{\omega m a_u}{\epsilon\Omega}v_{0t}\sin\xi'\right]=\sin\left[\Phi-\frac{\omega m a_u}{\epsilon\Omega}v_{0y}\right]J_0\left[\frac{m\omega a_u v_{0t}}{\epsilon\Omega}\right], \tag{A2}$$

where $v_{0t}=\sqrt{v_{0x}^2+v_{0y}^2}$ is the magnitude of the transverse velocity of the particle [see Eq. (8)]. The v_{0y} dependence in Eq. (A2) is an artifact appearing in the intermediate stage of our calculations. Because of the azimuthal symmetry of the problem, it will disappear after a proper averaging over all possible trajectories, as is done in Sec. III.

APPENDIX B: TRANSFORMATION OF EQ. (29)

To perform the transformation, it is convenient to use an integral representation of the zeroth order Bessel function J_0 [19],

$$J_0(\kappa\sqrt{x^2+y^2})=\frac{1}{\pi}\int_{-\kappa}^{\kappa} d\xi\, e^{i\xi y}\frac{\cos(x\sqrt{\kappa^2-\xi^2})}{\sqrt{\kappa^2-\xi^2}}. \tag{B1}$$

Having defined

$$\kappa\equiv\frac{\omega a_u}{\gamma_i\Omega}$$

and using Eq. (B1), one obtains for the integral over transverse velocity space in Eq. (29)

$$I(z,\tau)\equiv\frac{1}{(4qz+\theta_0^2)\sinh(\sqrt{2i\omega q}\,\tau)}\left[\frac{i\omega}{8q}\right]^{1/2}\int d^2v_t\exp\left[-\frac{v_t^2}{4qz+\theta_0^2}\right]J_0(\kappa v_t)$$

$$\times\int d^2v_t'\exp[-i\kappa(v_y'-v_y)]J_0(\kappa v_t')$$

$$\times\exp\left[\left[\frac{i\omega}{8q}\right]^{1/2}\left[\frac{2\mathbf{v}_t\cdot\mathbf{v}_t'}{\sinh(\sqrt{2i\omega q}\,\tau)}-[v_t^2+(v_t')^2]\coth(\sqrt{2i\omega q}\,\tau)\right]\right]$$

$$=\frac{1}{(4qz+\theta_0^2)\sinh(\sqrt{2i\omega q}\,\tau)}\left[\frac{i\omega}{8q}\right]^{1/2}\frac{1}{(2\pi)^2}\int_{-\kappa}^{\kappa}\frac{d\xi}{\sqrt{\kappa^2-\xi^2}}\int_{-\kappa}^{\kappa}\frac{d\eta}{\sqrt{\kappa^2-\eta^2}}$$

$$\times\int d^2v_t\int d^2v_t'\exp[-Av_t^2-B(v_t')^2+2C\mathbf{v}_t\cdot\mathbf{v}_t'+i(\kappa-\xi)v_y-i(\kappa-\eta)v_y']$$

$$\times(e^{iv_x\sqrt{\kappa^2-\xi^2}}+e^{-v_x\sqrt{\kappa^2-\xi^2}})(e^{iv_x'\sqrt{\kappa^2-\eta^2}}+e^{-iv_x'\sqrt{\kappa^2-\eta^2}}),$$

where

$$A\equiv\frac{1}{4qz+\theta_0^2}+\left[\frac{i\omega}{8q}\right]^{1/2}\coth(\sqrt{2i\omega q}\,\tau),$$

$$B\equiv\left[\frac{i\omega}{8q}\right]^{1/2}\coth(\sqrt{2i\omega q}\,\tau),$$

and

$$C\equiv\frac{1}{\sinh(\sqrt{2i\omega q}\,\tau)}\left[\frac{i\omega}{8q}\right]^{1/2}$$

are constants introduced for shorter notation.

The integral may thus be reduced to the sum of four integrals of a Gaussian type; each of them can be calculated with the help of the following formula:

$$\int_{-\infty}^{\infty} dx \int_{-\infty}^{\infty} dy e^{-Ax^2-By^2+2Cxy+i\alpha_1 x+i\alpha_2 y} = \frac{\pi}{\sqrt{AB-C^2}} \exp\left[-\frac{A\alpha_2^2+B\alpha_1^2+2C\alpha_1\alpha_2}{4(AB-C^2)}\right] . \tag{B2}$$

The combination $(AB-C^2)$ is common for all the four integrals and is equal to

$$AB-C^2=\left[\frac{i\omega}{8q}\right]^{1/2} \frac{\cosh(\sqrt{2i\omega q}\,\tau)+\sqrt{2i\omega q}\,(z+\theta_0^2/4q)\sinh(\sqrt{2i\omega q}\,\tau)}{(4qz+\theta_0^2)\sinh(\sqrt{2i\omega q}\,\tau)} . \tag{B3}$$

Calculating the four Gaussian integrals and putting them together, one has

$$\begin{aligned} I(z,\tau)=&\int_{-\kappa}^{\kappa}\frac{d\xi}{\sqrt{\kappa^2-\xi^2}}\int_{-\kappa}^{\kappa}\frac{d\eta}{\sqrt{\kappa^2-\eta^2}}\frac{1}{[\cosh(\sqrt{2i\omega q}\,\tau)+\sqrt{2i\omega q}\,(z+\theta_0^2/4q)\sinh(\sqrt{2i\omega q}\,\tau)]} \\ &\times\exp\left[\frac{2q(z+\theta_0^2/4q)[\kappa(2\kappa-\eta-\xi)\cosh(\sqrt{2i\omega q}\,\tau)-(\kappa-\eta)(\kappa-\xi)]}{\cosh(\sqrt{2i\omega q}\,\tau)+\sqrt{2i\omega q}\,(z+\theta_0^2/4q)\sinh(\sqrt{2i\omega q}\,\tau)}\right] \\ &\times\exp\left[\left[\frac{2q}{i\omega}\right]^{1/2}\frac{\kappa(\kappa-\eta)\sinh(\sqrt{2i\omega q}\,\tau)}{\cosh(\sqrt{2i\omega q}\,\tau)+\sqrt{2i\omega q}\,(z+\theta_0^2/4q)\sinh(\sqrt{2i\omega q}\,\tau)}\right] \\ &\times\cosh\left[\frac{2q(z+\theta_0^2/4q)\sqrt{(\kappa^2-\eta^2)(\kappa^2-\xi^2)}}{\cosh(\sqrt{2i\omega q}\,\tau)+\sqrt{2i\omega q}\,(z+\theta_0^2/4q)\sinh(\sqrt{2i\omega q}\,\tau)}\right] . \end{aligned} \tag{B4}$$

Substituting the above result into Eq. (29) and introducing new variables $\eta=\kappa\cos\phi$, $\xi=\kappa\cos\psi$, $\tau=t/\sqrt{\omega q}$, and $z=T/\sqrt{\omega q}-\theta_0^2/4q$, we arrive at our final formula Eq. (34).

[1] C. A. Brau, *Free-Electron Lasers* (Academic, New York, 1990).

[2] *Free Electron Lasers and Other Advanced Sources of Light—Scientific Research Opportunities* (National Academy Press, Washington, DC, 1994).

[3] A.-M. Fauchet, J. Feinstein, A. Gover, and R. H. Pantell, IEEE J. Quantum Electron. **QE-20**, 1332 (1984).

[4] J. Feinstein, A. S. Fisher, M. B. Reid, A. Ho, M. Özcan, H. D. Dulman, and R. H. Pantell, Phys. Rev. Lett. **60**, 18 (1988).

[5] R. H. Pantell, A. S. Fisher, J. Feinstein, A. Ho, M. Özcan, and H. D. Dulman, J. Opt. Soc. Am. B **6**, 1008 (1989).

[6] M. Özcan, R. H. Pantell, J. Feinstein, and A. H. Ho, IEEE J. Quantum Electron. **QE-27**, 171 (1991).

[7] M. B. Reid, J. Feinstein, R. H. Pantell, and A. S. Fisher, IEEE J. Quantum Electron. **QE-23**, 1539 (1987).

[8] M. B. Reid, J. Feinstein, R. H. Pantell, and A. S. Fisher, Nucl. Instr. Meth. **A272**, 268 (1988).

[9] M. Özcan, R. H. Pantell, and J. Feinstein, Nucl. Instr. Methods Phys. Res. Sect. A **296**, 226 (1990).

[10] L. K. Grover, *New Concepts in Free-Electron Lasers*, Ph.D. thesis, Stanford University, 1984 (unpublished).

[11] M. Özcan, Ph.D. thesis, Stanford University, 1991 (unpublished).

[12] W. B. Colson, Phys. Lett. **64A**, 190 (1977).

[13] L. D. Landau and E. M. Lifshitz, *Course of Theoretical Physics*, Vol. 8 (Pergamon, London, 1960).

[14] A. B. Migdal, Phys. Rev. **103**, 1811 (1956).

[15] N. P. Kalashnikov, V. S. Remizovich, and M. I. Ryazanov, *Collisions of Fast Charged Particles in Solids* (Gordon and Breach, New York, 1985).

[16] P. Sprangle and R. A. Smith, Phys. Rev. A **21**, 293 (1980).

[17] R. L. Sheffield, R. H. Austin, K. C. D. Chan, S. M. Gierman, J. M. Kinross-Wright, S. H. Kong, D. C. Nguyen, S. J. Russell, and C. A. Timmer, Nucl. Instr. Methods Phys. Res. Sect. A **341**, 371 (1994).

[18] M. B. Reid, A. S. Fisher, J. Feinstein, A. Ho, M. Özcan, H. D. Dulman, Y. J. Lee, and R. H. Pantell, Phys. Rev. Lett. **62**, 249 (1989).

[19] I. M. Ryshik and I. S. Gradstein, *Tables of Series, Products and Integrals* (VEB Deutscher Verlag der Wissenschaften, Berlin, 1957).